Supporting Information

How Surface Potential Determines the Kinetics of the First Hole Transfer of Photocatalytic Water Oxidation

Matthias M. Waegele,[†] Xihan Chen,[†] David M. Herlihy,[†] and Tanja Cuk[*,†,‡]

Department of Chemistry, University of California, Berkeley, Berkeley, CA, and Chemical Sciences Division, Lawrence Berkeley National Laboratory, Berkeley, CA

E-mail: tanjacuk@berkeley.edu

[*]To whom correspondence should be addressed
[†]Department of Chemistry, University of California, Berkeley, Berkeley, CA
[‡]Chemical Sciences Division, Lawrence Berkeley National Laboratory, Berkeley, CA

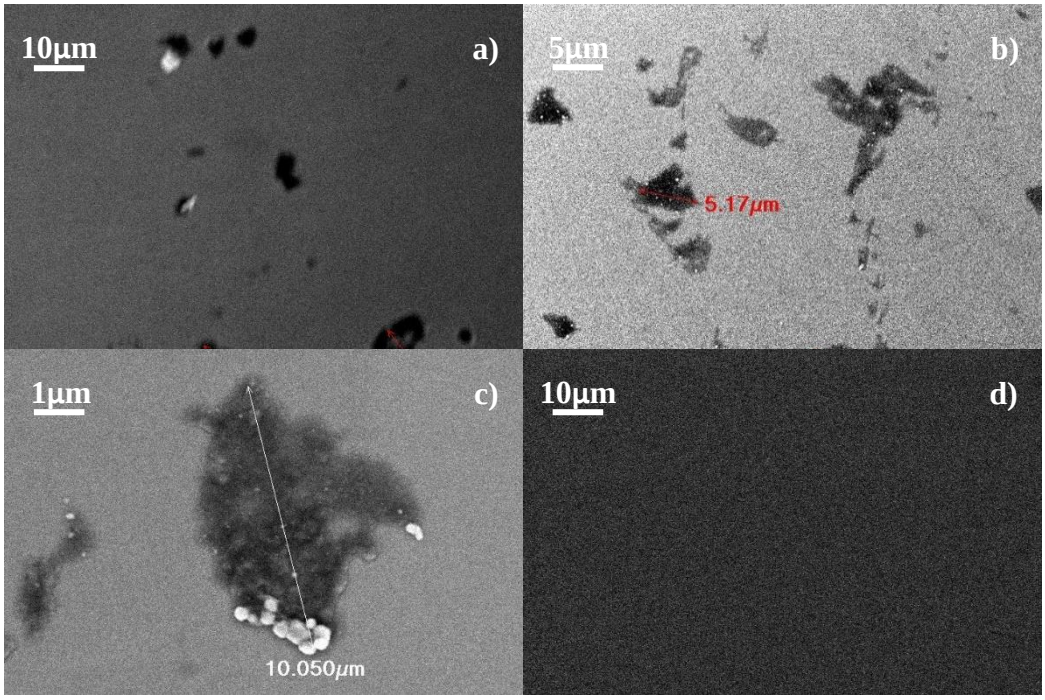

Fig. S 1: SEM images showing laser-induced damage on n-$SrTiO_3$. a) Damaged surface at 1500× magnification. b) Damaged surface of the same crystal at 2500× magnification, but at a different location. c) Higher magnification view (3500×) of two pits on the sample shown in b). d) Undamaged sample at 1500× magnification.

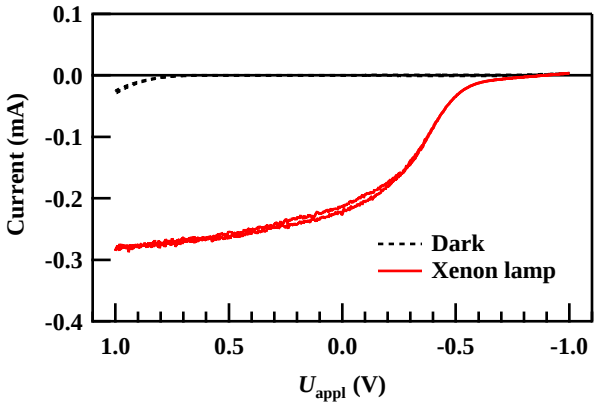

Fig. S 2: Cyclic voltammogram of n-$SrTiO_3$ in the dark and under irradiation by a 150 W Xenon lamp. Similar to the current-voltage curve under laser irradiation (Figure 1a of the main text), a diode-like behavior was observed under Xenon lamp irradiation. Note that compared to the data in Figure 1a, the photo-current is less potential independent in the range of -0.5 V to 1 V. The reason for this is that under Xenon lamp irradiation, a broad range of UV wavelengths was used, all with separate efficiencies for generating photocurrent. Further, the cathodic (dark) current relative to the photocurrent is much smaller in this figure. The reason for this is that the focal spot of the laser on the sample excited only $\pi \times 250^2$ μm^2 of the n-$SrTiO_3$ surface, whereas the Xenon lamp irradiated the entire 25 mm^2 surface, thereby producing a photocurrent that was much larger than the cathodic (dark) current.

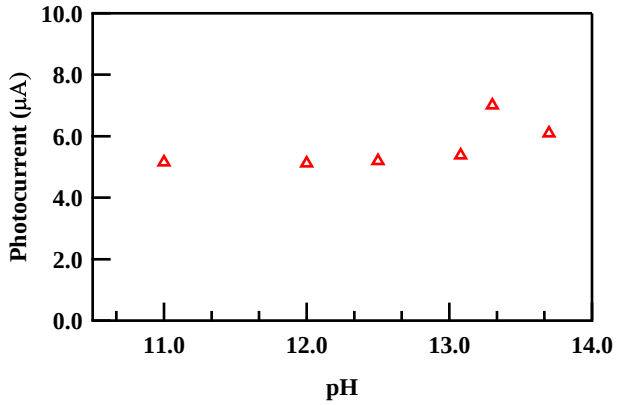

Fig. S 3: Steady state photocurrent of n-$SrTiO_3$ under an incident laser fluence of 0.04 mJ/cm^2 as a function of pH. The steady state photocurrent is not changing significantly with the pH of the solution, suggesting the reaction is not mass diffusion limited.

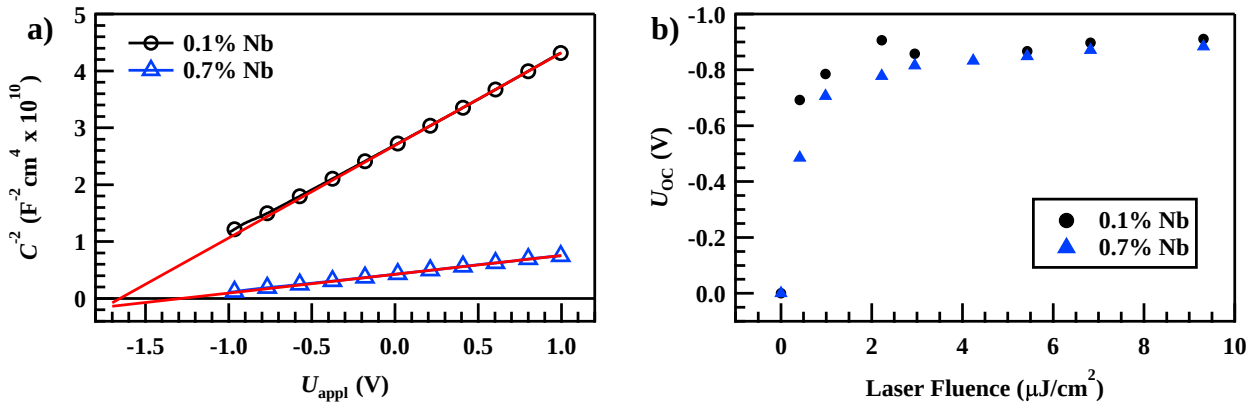

Fig. S 4: a) Mott-Schottky plots of n-$SrTiO_3$ in the dark. b) Photovoltage measurements of n-$SrTiO_3$ with laser irradiation. The graph indicates that only 2 μJ/cm^2 fluence is needed to flatten the semiconductor energy band. Determination of U_{fb}, U_{SC}, U_{H}, and C_{H} from these measurements is described below.

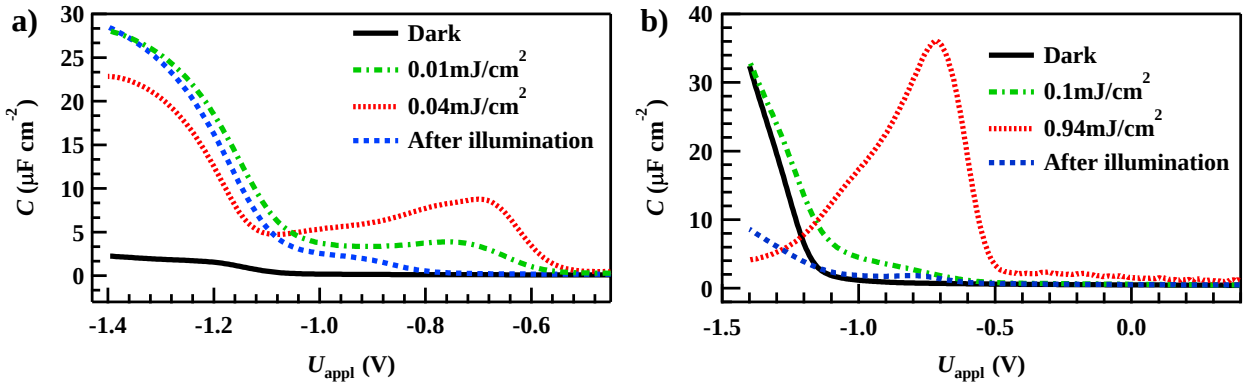

Fig. S 5: Differential capacitances of 0.1%Nb and 0.7% Nb-doped $SrTiO_3$ in an aqueous solution of 0.1 M Na_2SO_4, adjusted to a pH of 8.4 with NaOH, with and without laser irradiation as indicated. The photocurrent onsets at ≈ -0.85 V. As shown, capacitance changes dramatically upon light excitation which is an indication of carrier inversion that turns the surface of the n-type semicondutor into p-type. While carrier inversion was observed in both samples, a ≈ 10 times higher laser fluence was needed to achieve inversion in the more highly doped sample, consistent with the condition for carrier inversion, which is a photo-generated carrier density larger or equal to the semiconductor doping density.

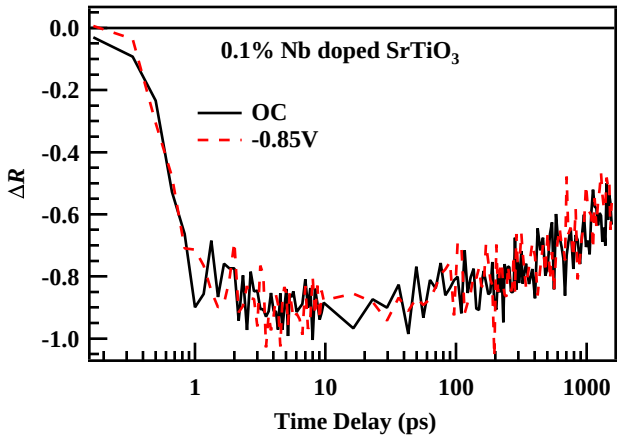

Fig. S 6: Comparison of transient reflectance traces for 0.1% Nb-doped $SrTiO_3$ under open circuit conditions and with an applied bias of −0.85 V. The invariance of the kinetics arises from identical surface hole potentials for the two cases as described in the main text.

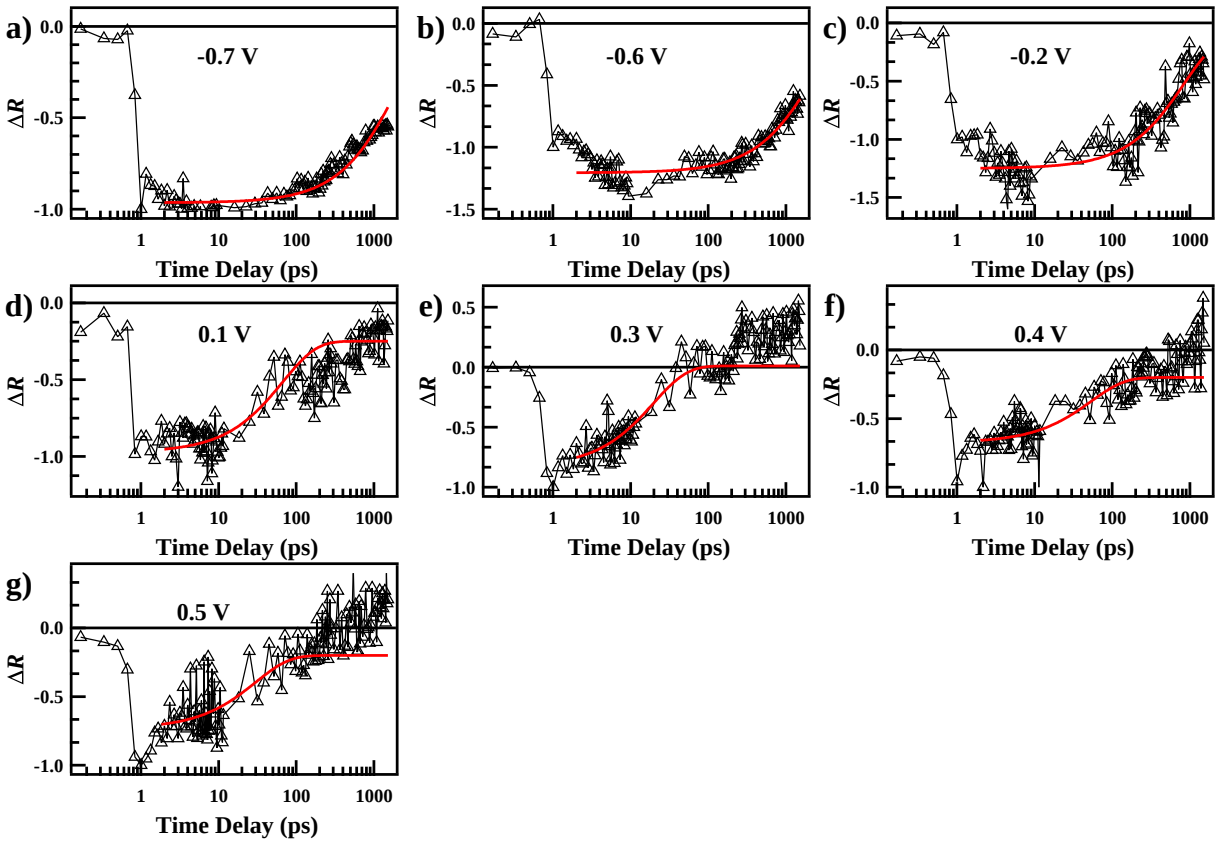

Fig. S 7: Normalized transient reflectance changes, attributed to the decay of photo-generated holes, probed at 800 nm at the specified U_{appl}. The data in this figure and the one shown in Figure 6a-e of the main text form the complete data set which was used to construct Figure 6f of the main text.

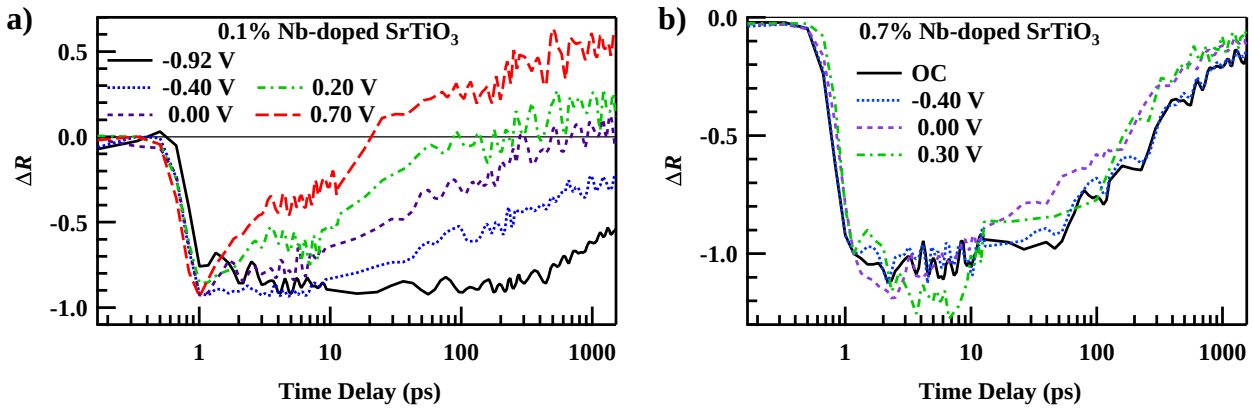

Fig. S 8: a) Same transient reflectance traces as in Figure 6 of the main text, but plotted on the same graph for direct comparison. b) Independence of the transient reflectance traces for 0.7% Nb-doped $SrTiO_3$ on applied potential. This independence is attributed to the lack of surface sensitivity of the probe in this sample as described in the main text.

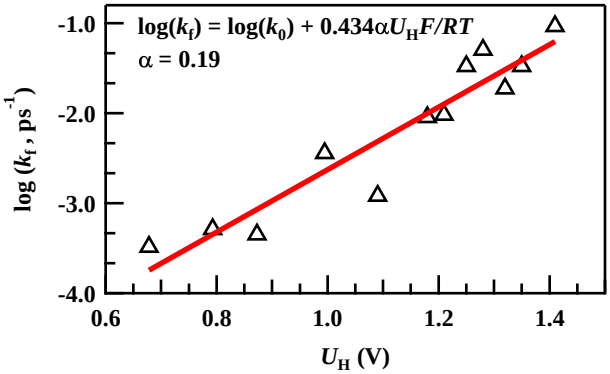

Fig. S 9: Plot of $\log(k_f)$ vs Helmholtz potential drop (U_H) as in Figure 7 of the main text, but based on an U_H which was calculated using an excitation fluence of 0.065 mJ cm^{-2}. The derived value of α is similar to the one obtained when using a fluence of 0.045 mJ cm^{-2}, indicating the robustness of the derived value to experimental uncertainties related to the absolute value of the fluence. The extracted value for k_0 is $(7.90 \pm 1.00) \times 10^{-7}$ ps^{-1}. The red line is a linear fit to the data.

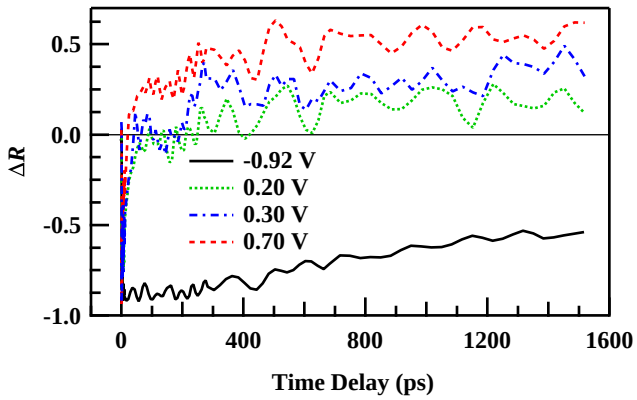

Fig. S 10: Representative transient reflectance traces of the same experiment shown in Figure 6 of the main text, but plotted on a linear time scale to emphasize the emergence of a transient signal of opposite sign under large reverse bias values. The signal changes sign at pump-probe time delay values < 200 ps. The persistence of this component beyond the observation window (≈ 1.5 ns) indicates the multi-component nature of the reaction kinetics.

Determination of the Helmholtz Capacitance and the Potential Distribution across the Semiconductor/Water Junction in the Dark

This section describes the procedure for determining the potential distribution across the semiconductor/water junction in the dark. A detailed description of the equations and theoretical framework used here can be found in (De Gryse *et al.* (1975) *J. Electrochem. Soc.* 122, 711 and Uosaki *et al.* (1983) *J. Electrochem. Soc.* 130, 895). The open-circuit photovoltage was measured as a function of laser fluence. As shown in Figure S4b, the photovoltage quickly saturates at higher light intensities to a value of -0.85 V. This saturation value is a direct measure of the band bending inside the semiconductor (U_{SC}). The charge stored in the depletion layer for this value of band bending is defined by equation (6) of the main text. This charge determines the potential drop across the Helmholtz layer:

$$U_{\mathrm{H}} = \frac{q_{\mathrm{SC}}}{C_{\mathrm{H}}} \tag{1}$$

For a highly doped semiconductor, as considered in the present case, the measured capacitance depends on both the depletion layer and Helmholtz capacitances, i.e. $\frac{1}{C} = \frac{1}{C_{\mathrm{SC}}} + \frac{1}{C_{\mathrm{H}}}$. The data in Figure S4a is further described by the Mott-Schottky equation:

$$\frac{1}{C^2} = \frac{1}{C_{\mathrm{H}}^2}\left\{1 + \frac{2C_{\mathrm{H}}^2}{e_0 \epsilon \epsilon_0 N_{\mathrm{d}}}\left(U - U_{\mathrm{fb}} - \frac{kT}{e_0}\right)\right\} \tag{2}$$

The relationship of the flatband potential (U_{fb}) and the x-intercept ($U_{C^{-2}=0} = -1.65$ V) of the Mott-Schottky plot (Figure S4a) is derived from equation 2:

$$U_{C^{-2}=0} = U_{\mathrm{fb}} + \frac{kT}{e_0} - \frac{e_0 \epsilon \epsilon_0 N_{\mathrm{d}}}{2C_{\mathrm{H}}^2} \tag{3}$$

We further have:

$$U_{\mathrm{appl}} - U_{\mathrm{fb}} = U_{\mathrm{H}} + U_{\mathrm{SC}} \tag{4}$$

Under equilibrium conditions, the only voltage drop across the semiconductor/electrolyte junction is $|U_{\mathrm{fb}}|$, which implies $U_{\mathrm{appl}} = 0$ V in equation 4. Inserting equations 1 and 3 into equation 4 and setting $U_{\mathrm{appl}} = 0$ V, we find $C_{\mathrm{H}} = 21$ μF/cm^2, $U_{\mathrm{H}} = 0.67$ V, and $U_{\mathrm{fb}} = -1.52$ V.

Differential Capacitance under Laser Light Excitation

This section interprets the measurements shown in Figure S5. Intense light excitation produces a large number of holes at the semiconductor surface. These photo-induced charges alter the distribution of the voltage drop across C_{SC} and C_{H}. To examine this effect, the total capacitance ($\frac{1}{C} = \frac{1}{C_{\mathrm{SC}}} + \frac{1}{C_{\mathrm{H}}}$) as a function of laser fluence was recorded in a voltage range above $U_{\mathrm{fb}} = -1.52$ V and below the onset of photocurrent (-0.85 V). For this set of measurements, an aqueous solution of 0.1 M Na_2SO_4, adjusted to a pH of 8.4 with NaOH, was used as the electrolyte. In this voltage range and electrolyte, the measured capacitance is solely due to the charging and discharging of the depletion layer and Helmholtz capacitances (C_{SC} and C_{H}, respectively), and not due to capacitances associated with sustained chemical reactions at the electrode surface (Faradaic capacitance).

Figure S5 shows the capacitance for several incident laser fluences. In the dark, the capacitance decreases with anodic voltage, as expected for reverse bias conditions that increase the depletion width. We observed characteristic changes in the capacitance that are only present during illumination and are clearly intensity dependent. Under light excitation, the capacitance also decreases, but only up to a certain intermediate anodic voltage where it begins to increase. The increasing capacitance is a mark of forward bias conditions, where the depletion width decreases with anodic voltages. These forward bias conditions are attributed to a large density of photo-induced holes that invert the native n-type band bending

into a very thin, p-type depletion layer at the semiconductor/electrolyte interface (Figure 3a of the main text).

Determination of the Nernstian Potential for the $OH^-/OH^\bullet$ Pair and the Overpotential for Water Oxidation

Overpotential for Water Oxidation

The voltage drop across the Helmholtz layer under illumination and applied voltage, $U_{\mathrm{H}}(U_{\mathrm{appl}})$, determines the valence band edge potential at the interface, and consequently the over-potential for O_2 evolution, as shown in Figure 4b of the main text. The valence band edge potential $\phi_{\mathrm{BE}}(U_{\mathrm{appl}})$ and over-potential η are defined by:

$$\phi_{\mathrm{BE}}(U_{\mathrm{appl}}) = \phi_{\mathrm{BE}}(U_{\mathrm{appl}} = 0) - U_{\mathrm{H}}(U_{\mathrm{appl}} = 0) + U_{\mathrm{H}}(U_{\mathrm{appl}}) \tag{5}$$

$$\eta = \phi_{\mathrm{BE}}(U_{\mathrm{appl}}) - \phi_{\mathrm{OH^-/O_2}} \tag{6}$$

$\phi_{\mathrm{BE}}(U_{\mathrm{appl}})$ was calculated from $\phi_{\mathrm{BE}}(U_{\mathrm{appl}} = 0) = 1.88$ V (at pH=13 vs NHE), the valence band edge potential at no applied potential and in the dark (Xu and Schoonen (2000) *Am. Mineral.* 85, 543), $U_{\mathrm{H}}(U_{\mathrm{appl}} = 0) = 0.67$ V, the Helmholtz voltage drop at no applied potential and in the dark (see previous section), and $U_{\mathrm{H}}(U_{\mathrm{appl}})$ the Helmholtz voltage drop at a given laser illumination, which was taken from Figure 4a of the main text. Note that within the employed theoretical framework, the Helmholtz voltage drop is only due the presence of the depletion layer in the semiconductor and photo-induced holes at its surface (equation (5) of the main text). The theory does not take into account the small fraction of the Helmholtz voltage drop that arises from the acid/base equilibrium at the semiconductor surface (van de Krol and Grätzel (2012) *Photoelectrochemical Hydrogen Production*, 102,

13-67; Springer: New York, NY).

Using $\phi_{OH^-/O_2} = +0.463$ V, the Nernstian potential for the water oxidation reaction at pH=13, the overpotential η was calculated. In Figure 4a of the main text, we show $U_H(U_{appl})$ on the left axis and the corresponding η on the right axis.

Nernstian Potential for the $OH^-/OH^\bullet$ Pair

In addition to considering the overpotential of the water oxidation reaction, the Nernstian potential for the $OH^-/OH^\bullet$ was calculated, which is physically more meaningful quantity in the context of the present measurements. As shown in Figure 4b of the main text, the Nernstian potential $\phi_{OH^-/OH^\bullet}$ is defined in the following way:

$$U_H(U_{app} = 0) = \phi_{BE}(U_{appl} = 0) - \phi_{OH^-/OH^\bullet} \tag{7}$$

Therefore, the Nernstian potential $\phi_{OH^-/OH^\bullet}$ is +1.21 V vs NHE at pH=13.

Determination of Hole Drift Time across the Depletion Region under Open Circuit Conditions

This section describes the procedure for determining the drift time of photo-generated holes across the depletion region. A detailed description of the equations and theoretical framework used here can be found in (Sze *et al.* (1985) *Semiconductor Devices Physics and Technology*, Wiley: New York, NY). In the semiconductor depletion region, the magnitude of the maximum of the electric field is given by:

$$E_m = \left(\frac{2e_0 N_d U_{SC}}{\epsilon_0 \epsilon}\right)^{1/2} \tag{8}$$

where N_d, ϵ_0, ϵ, e_0, represent the doping density, the vacuum permittivity, the dielectric constant of the semiconductor, and the electronic charge, respectively. For a value of $U_{SC} =$

0.85 V, we find $E_{\mathrm{m}} \approx 450$ kV/cm. The maximum carrier drift velocity is given by:

$$v_{\mathrm{d}} = \mu E_{\mathrm{m}} \tag{9}$$

The carrier mobility μ is 5.5 $\mathrm{cm}^2/\mathrm{V\ s}$ (Tufte *et al.* (1967) *Phys. Rev* 155, 796), giving a maximum drift velocity of 2.5×10^6 cm/s. As the electric field is linear in the depletion region, the average hole drift velocity is approximately half of its maximum value. For a depletion width of 25 nm, the hole drift time out of depletion region is estimated to be 2 ps.